

# Sound Absorption by Subwavelength Membrane Structures: A Generalized Perspective

Min Yang,<sup>1</sup> Yong Li,<sup>1</sup> Chong Meng,<sup>1</sup> Caixing Fu,<sup>1</sup> Jun Mei,<sup>2</sup> Zhiyu Yang,<sup>1</sup> and Ping Sheng<sup>1,\*</sup>

<sup>1</sup>*Department of Physics, Hong Kong University of Science and Technology, Clear Water Bay, Kowloon, Hong Kong, China*

<sup>2</sup>*Department of Physics, South China University of Technology, Guangzhou 510640, China*

Decorated membrane, comprising a thin layer of elastic film with small rigid platelets fixed on top, has been found to be an efficient absorber of low frequency sound. In this work we consider the problem of sound absorption from a perspective aimed at deriving upper bounds under different scenarios, i.e., whether the sound is incident from one side only or from both sides, and whether there is a reflecting surface on the back side of the membrane. By considering the negligible thickness of the membrane, usually on the order of a fraction of one millimeter, we derive a relation showing that the sum of the incoming sound waves' (complex) pressure amplitudes, averaged over the area of the membrane, must be equal to that of the outgoing waves. By using this relation, and without going to any details of the wave solutions, it is shown that the maximum absorption achievable from one-side incident is 50%, while the maximum absorption with a back reflecting surface can reach 100%. The latter was attained by the hybridized resonances. All the results are shown to be in excellent agreement with the experiments. This generalized perspective, when used together with the Green function formalism, can be useful in gaining insights and delineating the constraints on what are achievable in scatterings and absorption by thin film structures.

PACS numbers: 42.25.Bs, 43.20.+g, 43.40.+s, 43.55.Ev, 46.40.-f, 62.30.+d

## I. INTRODUCTION

A sound absorber converts the airborne acoustic energy into thermal motions via irreversible processes. High efficiency of such processes requires not only properly matched impedance for the absorber, but also the dissipative ability to absorb the incident energy. Traditional means of acoustic absorption make use of porous and fibrous materials [1], gradient index materials, or perforated panels [2] with tuned cavity depth behind the panels. They generally result in either imperfect impedance matching to the incoming wave, or very bulky structures with dimensions comparable to the wavelength, usually on the order of meters for low frequency airborne sound.

Membrane-type acoustic metamaterial, consisting of decorated membrane resonator (DMR) of various forms, has been shown to display diverse functionalities such as efficient reflection [3–7], enhanced transmission [8], reversed Doppler effect [9], and near-field amplification [10]. The reason for such extraordinary behaviors can be attributed to the effective negative mass density [3, 11] and/or negative refractive index [12, 13] introduced by the DMR's subwavelength resonances. Recent works also show that the DMR can efficiently absorb low frequency sound even with its negligible thickness [14, 15], a capability clearly beyond what is achievable by conventional acoustic absorbers. This has been attributed to the high energy density of DMR's lateral resonances. Hybridization of different resonances can even lead to perfect absorptions in the deep-subwavelength regime, thereby realizing the exact time-reversed counterpart of an acoustic point source [16]. The latter is known to have important applications for time-reversal wave technology [17]. By using hybridized modes, an acoustic metasurface can be realized with

an array of such acoustic “sinks” with extraordinary sound absorption characteristics [18].

In this work, we present a generalized perspective, based on DMR's special geometric characteristic, for understanding DMR's sound absorption behaviors. It is shown that, owing to membrane's negligible thickness, there is an equality relating the sum of mean complex pressure amplitudes (MCPA) of the incoming waves, averaged over the area of DMR, to that of the outgoing waves. By drawing analogy to momentum conservation law involving two equal-mass particles, it is easily seen that there is a component of the total incident energy, corresponding to the center of mass motion in the two particles collision, which is always conserved and therefore cannot be dissipated. Hence only the energy in excess of the conserved component is available for dissipation. This observation leads to upper limits for DMR's absorption performance under various scenarios. In particular, for wave incident from one side only, only half of the incoming energy is available for dissipation, thus the absorption percentage cannot exceed 50% [15]. We verify this conclusion by experimentally observing the sound scattering from DMRs, and the results show excellent agreement with theoretical predictions. Such general considerations also show that the higher than 50% absorption can be achieved either by allowing waves to be incident from both sides of the membrane, such as in the coherent perfect absorption (CPA) scenario [19], or if multiple scatterings are introduced into the system by introducing a back reflecting surface. As an example, the acoustic metasurface with hybrid resonances, which has been demonstrated to completely absorb waves incident from one side, is analyzed in light of the MCPA conservation. The outcome, while matching the results previously reported [18], also yields additional insights.

In what follows, Section II shows how the area-averaged response of a subwavelength membrane structure can be reduced to a one-dimensional problem, and the related physics, as embedded in the Green function formalism, is considerably simplified as a result. In Section III we derive a general

---

\* Correspondence email: sheng@ust.hk

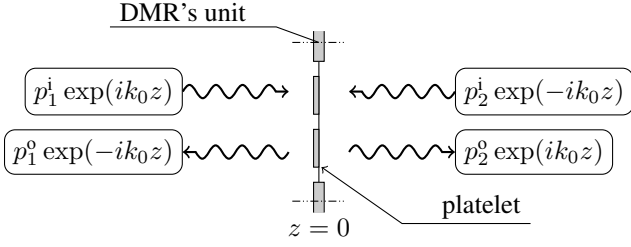


FIG. 1. Schematic illustration of the scattering process from a DMR's unit. With left-incident sound wave's pressure denoted as  $p_1^i \exp(ik_0z)$  and that from the right as  $p_2^i \exp(-ik_0z)$ , the scattering generates two outgoing waves  $p_1^o \exp(-ik_0z)$  and  $p_2^o \exp(ik_0z)$ . Here  $k_0$  is the sound wave's wavevector in air, and the double dot-dash lines stand for periodic boundary conditions. According to the conservation of mean complex pressure amplitude (MCPA),  $p_1^i + p_2^i = p_1^o + p_2^o$ .

conservation rule governing the scatterings from thin membrane structures, and show how some conclusions can be easily derived from this rule without having to resort to the wave equation. In Section IV we analyze the problem of an efficient thin membrane absorber using the generalized perspective, and verify experimentally the derived conservation rule. In Section V the problem of a membrane resonator coupled to a thin, sealed air cell is analyzed, leading to the condition for attaining perfect absorption through hybrid resonances. This is followed by a brief summary in Section VI that concludes the article. In the Appendix we derive the formulas for obtaining the theoretically relevant parameters from four-probe impedance tube data.

## II. SURFACE IMPEDANCE AND DISSIPATION

A DMR unit comprises a uniformly stretched elastic membrane decorated with relatively rigid platelets. It is important for our subsequent considerations to note that the thickness of the membrane is negligible ( $\sim 200 \mu\text{m}$ ), while the cross-sectional dimension of the membrane is subwavelength in scale for the frequency regime of interest. Without the loss of generality, we can consider it as an inhomogeneous membrane which can vibrate and scatter the incoming plane waves as shown in Fig. 1.

Central to the understanding of DMR's acoustic behaviors is that only the piston-like component of its averaged displacement,  $\langle W \rangle$ , couples to the radiative wave modes. Here  $W$  denotes the normal displacement field of the membrane, and the angular bracket denotes surface averaging. However, the variance of the displacement,  $\delta W \equiv W - \langle W \rangle$ , is decoupled from the radiation modes and can be characterized as "deaf". The reason of this decoupling can be seen from the Fourier wavevectors  $\mathbf{k}_{\parallel}$  that delineate the lateral spatial pattern of  $W$ . For the  $\delta W$ , the relevant  $\mathbf{k}$  must have magnitude that satisfy the inequality  $|\mathbf{k}_{\parallel}| > 2\pi/\lambda$ , where  $\lambda$  is the sound wavelength in air, owing to membrane's subwavelength cross-sectional dimension. From the displacement continuity condition and the wave dispersion relation, we have  $(k_{\parallel})^2 + (k_{\perp})^2 = (2\pi/\lambda)^2$

for the acoustic wave in air, where  $k_{\perp}$  denotes the wavevector component normal to the membrane. It follows that the  $\delta W$  component couples only to the evanescent waves, as its associated  $k_{\perp}$  must be imaginary. In contrast, because the  $\mathbf{k}_{\parallel}$  components for  $\langle W \rangle$  have a distribution that peaks at  $\mathbf{k}_{\parallel} = 0$ , it can couple to the radiation modes. Hence, if we restrict our considerations to only the radiation modes, then one can treat the problem of DMR as essentially one-dimensional in character.

The surface impedance, which characterizes the DMR's far-field scattering properties, can be defined by using only the  $\langle W \rangle$  component, given by  $Z = \langle p \rangle / \langle \dot{W} \rangle$ , with  $p$  denoting the total sound pressure acting on the membrane and the over-dot denoting the time derivative. We notice that, for harmonically oscillating waves with angular frequency  $\omega = 2\pi f$ , the time-averaged energy flux pointing into the membrane (which characterizes the energy dissipation rate by the membrane) is given by  $j = \int_0^{2\pi} \text{Re}(\langle p \rangle e^{-i\omega t}) \text{Re}(\langle \dot{W} \rangle e^{-i\omega t}) d(\omega t) / (2\pi)$  [20]. Since the surface impedance's real part,  $\text{Re}(Z)$ , results from the velocity component with the same phase as pressure, hence this is the component that characterizes DMR's dissipative capability. It follows that  $j = \langle p \rangle^2 \text{Re}(Z) / (2|Z|^2)$ . This dissipation is caused by the viscous damping in membrane's relative displacements. In particular, the displacements in the "deaf" component  $\delta W$  dominate dissipation. Therefore, there is a relation between  $\text{Re}(Z)$  and  $\delta W$  as shown explicitly in what follows.

The surface-averaged Green function is defined by  $\langle G \rangle = \langle W \rangle / \langle p \rangle$ . Hence, for time-harmonic motion, we have  $Z = i / (\omega \langle G \rangle)$ . For frequencies in the vicinity of one of DMR's resonances,  $\langle G \rangle$  is given by [21]

$$\langle G \rangle = \frac{|W_n\rangle^2}{\rho_n(\omega_n^2 - \omega^2 - 2i\omega\beta_n)}, \quad (1)$$

where  $\rho_n \equiv \int_{\Omega} \rho |W_n|^2 dV$  is a parameter related to the displacement-weighted mass density for the membrane's  $n$ th eigenmode  $W_n$ ,  $\rho$  is the local mass density,  $\Omega$  the volume of the membrane, and  $\omega_n$  is the relevant angular eigenfrequency. If we denote the viscosity coefficient of the membrane as  $\eta$  [22], then the dissipation coefficient  $\beta_n$  in Eq. (1) is defined by

$$\begin{aligned} \beta_n &\equiv \int_{\Omega} \eta (\nabla W_n^* \cdot \nabla W_n) dV / (2\rho_n) \\ &= \int_{\Omega} \eta (\nabla \delta W_n^* \cdot \nabla \delta W_n) dV / (2\rho_n), \end{aligned} \quad (2)$$

In Eq. (2) we have used the fact that  $\nabla \langle W_n \rangle = 0$ . It follows that the relevant impedance corresponding to frequencies in the vicinity of a resonance is given by

$$Z = \frac{i}{\omega \langle G \rangle} = \frac{\rho_n}{|W_n\rangle^2} \left[ 2\beta_n + \frac{i}{\omega} (\omega_n^2 - \omega^2) \right]. \quad (3)$$

Equations (2) and (3) indicate that, although decoupled from radiation modes, the "deaf" component  $\delta W$  can still affect scatterings via membrane's dissipation coefficient  $\beta_n$ .

This can be accomplished through structural designs. For instance, decorating membrane with semicircular platelets can lead to “flapping” modes having a large  $\delta W$  component and hence large dissipation [14]. However, a large dissipation sometimes may also cause impedance mismatching, thereby leading to reflection instead of absorption. Hence “sufficient” dissipation that is compatible with impedance matching is always the key to an efficient absorber.

### III. A RELATION INVOLVING THE MEAN COMPLEX PRESSURE AMPLITUDES (MCPA)

In this section, we will look at the problem of thin membrane absorption through a different perspective. As shown in Fig. 1, the two incoming waves counter-propagate from two sides, acting on the DMR with complex pressures amplitudes  $p_1^i$  and  $p_2^i$ . After scattering, they are converted into two outgoing waves with complex pressure amplitudes  $p_1^o$  and  $p_2^o$ . Here, the subscript “1(2)” denotes the left (right)-hand side region and the superscript “i(o)” stands for incoming(outgoing) waves. Notice that the sound’s energy flux in air,  $j = \int_0^{2\pi} \text{Re}(pe^{-i\omega t})\text{Re}(\dot{W}e^{-i\omega t})d(\omega t)/(2\pi) = p\dot{W}/2 = \pm p^2/(2Z_0)$ , is opposite in directions for the incident and scattering waves. Here  $Z_0$  denotes the characteristic impedance of air. Therefore, the air’s surface-averaged normal velocities on two sides of the membrane are given by

$$\langle \dot{W}_1 \rangle = \frac{2j_1^i}{p_1^i} + \frac{2j_1^o}{p_1^o} = \frac{1}{Z_0}(p_1^i - p_1^o), \quad (4a)$$

$$\langle \dot{W}_2 \rangle = \frac{2j_2^o}{p_2^o} + \frac{2j_2^i}{p_2^i} = \frac{1}{Z_0}(p_2^o - p_2^i), \quad (4b)$$

respectively. Since the thickness of the membrane is negligible, we have  $\langle \dot{W}_1 \rangle = \langle \dot{W}_2 \rangle$ , i.e., there is no relative motion between the two sides of the membrane. That immediately implies that the mean complex pressure amplitude (MCPA),  $\bar{p}$ , is conserved before and after the scattering:

$$\bar{p} = \frac{1}{2}(p_1^i + p_2^i) = \frac{1}{2}(p_1^o + p_2^o). \quad (5)$$

Conservation of the MCPA implies that the portion of incoming energy associated with it has to be preserved from dissipation and transferred to radiative outgoing waves by scatterings. This is an direct analogy to the two (equal-mass) particles scattering in classical mechanics, if we regard the  $p$ ’s as momenta of the two particles before and after the collision. In that analogy Eq. (5) expresses the fact that the center of mass momentum is always conserved before and after the collision. For waves with amplitude  $p_1^i$  from left and  $p_2^i$  from right, the overall incoming energy flux is given by  $[(p_1^i)^2 + (p_2^i)^2]/(2Z_0)$ , while the conserved MCPA energy is simply  $\bar{p}^2/Z_0$ . The component of the total energy flux available for dissipation,  $\tilde{j}$ , must be the difference between the two, given by

$$\tilde{j} = (p_1^i - p_2^i)^2/(4Z_0). \quad (6)$$

If we denote the energy flux being absorbed as  $j_{ab}$ , then  $j_{ab} \leq \tilde{j}$  always, and the absorption coefficient,  $A = j_{ab}/(\tilde{j} + \bar{j})$ , has an upper bound of  $\tilde{j}/(\tilde{j} + \bar{j})$ .

Some easy conclusions can be stated immediately. First, if the incoming wave is from one side only, then  $p_2^i = 0$  and  $\bar{p} = p_1^i/2$ . It follows that  $\bar{j} = \tilde{j}$  and the absorption can at most be 50%. Second, for  $A = 1$ , i.e., perfect absorption, one must have  $\bar{j} = 0$ , which is only possible if  $p_1^i = -p_2^i$ , so that  $\bar{p} = 0$ . This corresponds to the CPA scenario [19]. In general, for a given ratio  $\alpha = |p_2^i|/|p_1^i|$ , the maximum absorption always occurs when  $p_1^i$  and  $p_2^i$  are opposite in phase, so that they can maximally cancel each other such that

$$\begin{aligned} A_{\max} &= \frac{\tilde{j}}{\bar{j} + \tilde{j}} = \frac{(p_1^i)^2 + (p_2^i)^2 + 2|p_1^i p_2^i|}{2(p_1^i)^2 + 2(p_2^i)^2} \\ &= \frac{1}{2} + \frac{\alpha}{1 + \alpha^2}. \end{aligned} \quad (7)$$

It is interesting to see under what condition(s) would  $\tilde{j}$  be completely dissipated when the condition of  $\alpha = 1$  is relaxed. That requires the total outgoing energy flux, given by  $[(p_1^o)^2 + (p_2^o)^2]/(2Z_0)$ , be equal to the conserved MCPA energy  $\bar{j} = \bar{p}^2/Z_0$ . This can occur when  $p_1^o = p_2^o = \bar{p}$ . Since the two outgoing waves are opposite in direction, their pressure exactly cancel each other on the membrane. Hence the net pressure on the membrane is given by  $\langle p_{\text{tot}} \rangle = p_1^i - p_2^i$ , while displacement continuity means that the membrane’s surface-averaged normal velocity  $\langle \dot{W} \rangle$  must be equal to that of air,  $\langle \dot{W}_1 \rangle$ , which is defined by Eq. (4a). Thus  $\langle \dot{W} \rangle = \langle \dot{W}_1 \rangle = (p_1^i - p_1^o)/Z_0 = (p_1^i - p_2^i)/(2Z_0)$  since  $p_1^o = \bar{p} = (p_1^i + p_2^i)/2$ . In other words, the requirement boils down to

$$Z = \langle p_{\text{tot}} \rangle / \langle \dot{W} \rangle = 2Z_0. \quad (8)$$

Therefore, as long as a DMR has a purely real surface impedance twice the impedance of air, it has the ability to absorb all the available energy  $\tilde{j}$  in the incoming waves. According to Eq. (3), such impedance is realizable at the resonances of a DMR, i.e., when  $\omega = \omega_n$ , with a suitably valued  $\beta_n$ .

### IV. DECORATED MEMBRANE WITH SEMICIRCULAR PLATELETS

In this and the following Sections, we shall present two scenarios involving large dissipation by the DMRs in which the absorption measurements are performed by using the setup shown in Fig. 2(a). In the present Section we consider absorption by DMRs with asymmetric platelets.

As the rubber membrane is usually weakly dissipative in character, we decorate it with semicircular platelets to utilize the high concentration of curvature energy at the edges of the platelets to enhance the dissipation. The asymmetry of the platelets means that there can be “flapping” modes [Figs. 2(c) and (d)] which represent a combination of normal displacement of the platelets in conjunction with a rotational motion. At the perimeters of the platelets, there can be very high concentration of so-called curvature energy that is proportional to

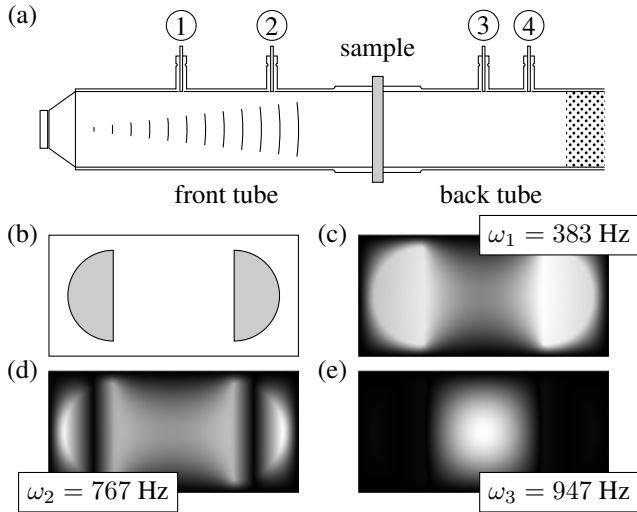


FIG. 2. (a) Schematic illustration of the experiment apparatus. The front tube with a loudspeaker at one end has two sensors, while the back tube having the other two sensors is plugged by acoustic foam at another end. These four sensors are marked from 1 to 4 in succession. (b-e) Front views of the DMR's structure and its eigenmodes' profiles. Decorated by two opposite semicircular platelets [gray semicircles in (b)], the stretched membrane [white rectangle in (b)] presents three eigenmodes below 1 kHz whose normal displacement amplitude  $|W|$  is plotted in gray scale as shown in (c-e).

the square of the second derivative of the normal displacement along the membrane surface directions. Since the energy dissipation is given by the integral of the product of energy density with the dissipation coefficient, a very high energy density can significantly enhance the absorption of sound. Moreover, with platelets of different weights, the size of this edge effect can be tuned to give different  $\text{Re}(Z)$ .

Fig. 2(b) shows a unit of our DMR. Four edges of the stretched rectangle membrane are fixed on a rigid frame. On top of the membrane, two decorated semicircular platelets are fixed to face each other. The membrane has a width of 15 mm, length of 30 mm, and a thickness of 0.2 mm. While the mass of platelets can vary in different samples, the radius for each platelet is kept at 6 mm.

We test the DMR's scattering and absorption properties by mounting a unit of the DMR on a rigid plate, and the whole sample is sandwiched by two impedance tubes having square cross-sections (see the inset in Fig. 3). The front tube has two sensors [Fig. 2(a)], plus a loudspeaker at the front end to generate the plane waves. The back tube has another two sensors, and the tube's back end is filled by acoustic foam to eliminate reflection. By normalizing the pressure amplitude of all the relevant sound waves by the incident sound pressure amplitude, the reflection and transmission coefficients,  $R$  and  $T$ , can be obtained from the pressure data recorded by the four sensors (see Eq. A5 in Appendix).

In the present case the incident wave is from one side only, hence in accordance to their definitions,  $R = p_1^o/p_1^i$  and  $T = p_2^o/p_1^i$ . The MCPA conservation in this case is given by the simple relation  $1 = R + T$  (notice that this is not the

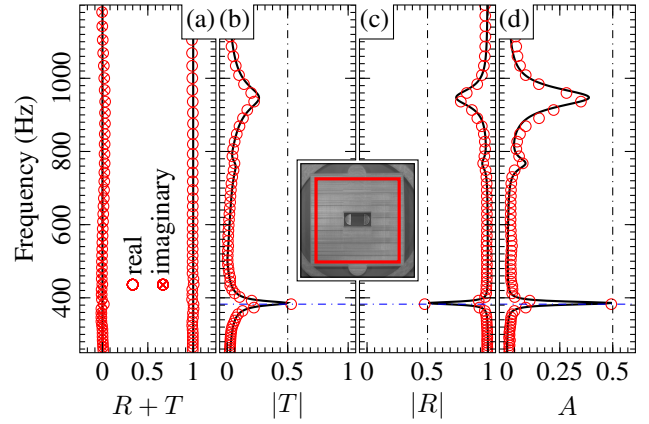


FIG. 3. Evidence of MCPA conservation and total absorption of available energy under one-side incident wave. (a) Small discrepancies between  $R + T$  and 1 ( $< 2.97\%$ ) confirm the conservation of MCPA. Equal amplitude, close to 0.5 for both  $T$  in (b) and  $R$  in (c) (only their magnitudes have been shown here for clarity) at 383 Hz, indicates all the available energy has been absorbed, as shown by the absorption peak of 49.327% at the same frequency in (d). The red circles are the experimental results, the black curves are calculated from the eigenmodes shown in Figs. 2(c-e). The inset shows the experimental sample with the red square indicating the area covered by the impedance tube.

energy conservation law, which would involve the square of  $R$  and  $T$ ). We can check it directly by comparing the measured values of  $R + T$  with 1. For a sample with identical platelets' mass of 151 mg each, Figs. 3(a-c) show the measured  $R + T$ ,  $|T|$ , and  $|R|$  respectively. The small discrepancy between  $R + T$  and 1 ( $< 2.97\%$ ) confirms the validity of the MCPA's conservation over *all* frequencies of interest.

We notice that, at the resonant frequency of 383 Hz, both  $R$  and  $T$  have an approximately equal value ( $\simeq 0.5$ ). It indicates an almost total absorption for the available energy  $\tilde{j}$  (which equals to the MCPA energy  $\tilde{j}$  here), hence the absorption coefficient  $A$  reaches its maximum value  $A_{\text{max}} = 0.5$  [i.e.,  $\alpha = 0$  in Eq. (7)]. This is seen from the measured absorption coefficient  $A = 1 - |R|^2 - |T|^2$  with a peak magnitude of  $\sim 0.493$  at the same frequency as shown in Fig. 3(d).

The displacement profile of this (maximum absorption) resonant mode is shown in Fig. 2(c) [together with Figs. 2(d) and (e) for the other two absorption peaks in Fig. 3(d)], which is numerically simulated (based on the material parameters in Ref. [21]) by using COMSOL Multiphysics—a commercial finite-element solver software. Based on this eigenmode, the evaluated parameter values from the experimental data are  $|\langle W_1 \rangle|^2/\rho_1 = 0.039 \text{ m}^2/\text{kg}$ ,  $\omega_1 = 2\pi \times 283.43 \text{ Hz}$ ,  $\beta_1 = 15.74 \text{ Hz}$  and  $\eta = 1.76 \text{ Pa}\cdot\text{s}$ . The surface impedance of this DMR can therefore be calculated by using Eq. (3) to yield  $Z = 1.986Z_0$ , which is very coincident with the condition as expressed by Eq. (8). Resonances' departures from this condition are caused by mismatching in impedance, thereby leading to weaker absorptions. We demonstrate this effect by 7 samples having platelets' mass varying from 34 to 825 mg, and comparing the peak absorption coefficient  $A_{\text{peak}}$  with the rel-

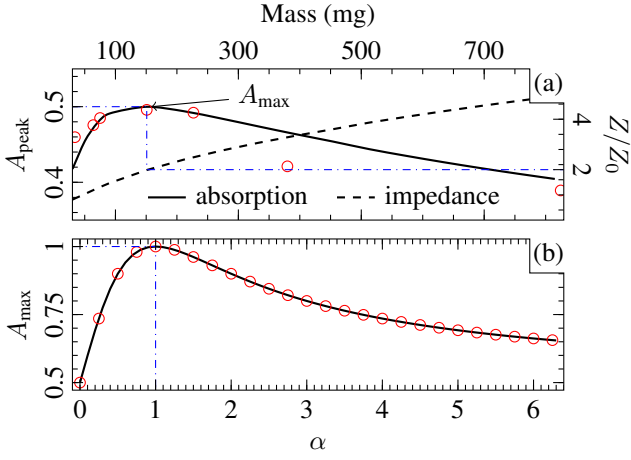


FIG. 4. Maximum absorption for impedance-matching and its relation with incident waves' symmetry. (a) To absorb one-side incident wave, the DMR samples with differently weighted platelets are shown to display various peak absorption coefficients  $A_{\text{peak}}$ , with the maximum achieved when the relevant impedance satisfies the condition as expressed by (8)— $Z = 2Z_0$ , with  $Z_0$  being the characteristic impedance of air. The black lines are from numerical simulations while the red circles denote experimental data. (b) Different maximum absorption coefficient  $A_{\text{max}}$  for two-side incident waves for various values of  $\alpha^2$ . The numerically simulated result (red circles) matches Eq. (7) (black curve) very well.

evant surface impedance in Fig. 4(a). Clearly, the maximum peak absorption is attained when the condition expressed by (8) is met.

Through numerical simulations, we further locate the maximum absorption coefficient  $A_{\text{max}}$  for two-side incoming waves with various values of  $\alpha^2 = |p_2^i|^2/|p_1^i|^2$ , by using the DMR with platelets' mass of 151 mg each. As shown in Fig. 4(b), almost perfect agreement between the numerically simulated results and that predicted by Eq. (7) is seen. This confirms again the validity of the ‘‘available energy for dissipation’’ concept, and its relation to MCPA.

Combinations of different units in one panel can give rise to a broader absorption spectrum. We demonstrate this by using a panel consisting of eight different units (see the inset of Fig. 5). Five of them have decorated platelets with mass of 225 mg each, and the other three have platelets with masses of 70, 140, and 445 mg. The experimentally measured absorption coefficient  $A$  for this panel is shown in Fig. 5. A relatively broad absorption spectrum [compared to that shown in Fig. 3(d)] is seen due to the merging of multiple absorption peaks. We would like to note here that none of the absorption spectra in Fig. 3(d) and Fig. 5 exceed 50%. In this context we would like to note that in Ref. [14], maximum absorption over 70% has been reported for a one-side incident wave configuration. The reason for this discrepancy is simply the absorption area. The DMR panel in Ref. [14] has a larger area (about 2.26 times larger) than the incoming wave front, and part of the sample extended outside of the impedance tube. Here, the tested samples are always contained within the impedance tube, and have exactly the same cross-section [see the insets

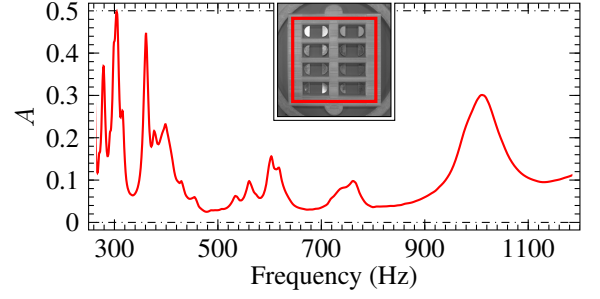


FIG. 5. Experimentally measured absorption spectrum for a DMR panel with 8 units. Five in these eight units have the same decorated semicircular platelets weighting 225 mg, while the other three platelets have masses of 70, 140, and 445 mg. The inset shows the experimental sample, in which the red square indicates the area covered by the impedance tube.

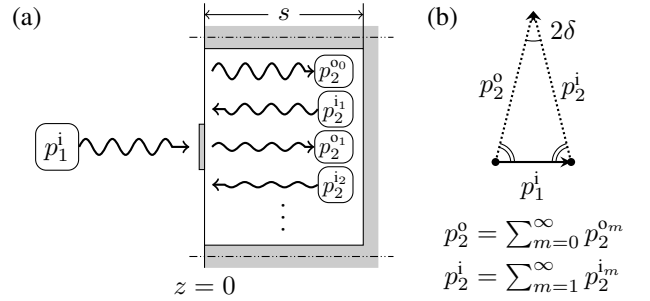


FIG. 6. Schematic illustration of the multiply-scattered waves that can lead to perfect absorption on a DMR, with a reflecting wall placed a small distance  $s$  behind it. (a) When the incoming wave energy has been totally absorbed, there should be no reflections, i.e., all the scatterings on the incident side cancel each other  $p_1^o \exp(-ik_0z) = \sum_{m=0}^{\infty} p_1^{om} \exp(-ik_0z) = 0$ . Incoming wave  $p_1^i \exp(ik_0z)$  generates only two net counter-propagating wave components  $p_2^o \exp(ik_0z) = \sum_{m=0}^{\infty} p_2^{om} \exp(ik_0z)$  and  $p_2^i \exp(-ik_0z) = \sum_{m=1}^{\infty} p_2^{im} \exp(-ik_0z)$ , in the air layer between the DMR (at  $z = 0$ ) and the reflecting wall. Here, the double dot-dash lines stand for the location at which the periodic boundary condition is applied. (b) Due to the MCPA conservation, the three complex pressure amplitudes must form an isosceles triangle whose two equal sides are slanted toward each other with an angle given by  $2\delta = 2k_0s$ .

in Fig. 3(d) and Fig. 5].

## V. PERFECT ABSORPTION BY ACOUSTIC METASURFACE

Although the MCPA energy in the incoming waves has to be conserved in a single scattering event, its dissipation is still possible through multiple scatterings. The outgoing MCPA energy after each scattering can serve as the incoming energy again for the subsequent scatterings. An example is the acoustic metasurface reported in Ref. [18], in which a reflecting wall is placed behind a DMR, separated by a distance  $s$  that is deeply subwavelength (2 orders smaller than the relevant

wavelength in air), thereby creating multiple reflections between the membrane and the reflecting wall [see in Fig. 6(a)]. As a result, the absorption coefficient for one-side incident wave can reach nearly 100%. In this section, we analyze this multiple-scattering process and the perfect absorption condition with the aid of MCPA conservation.

In the air layer between the membrane and the reflecting surface, the outgoing wave after the  $m$ th scattering from the membrane,  $p_2^{o_m}$ , is reflected by the wall, and becomes the incoming wave,  $p_2^{i_{m+1}}$ , for the  $(m+1)$ th scattering. These multiple scattered waves can be superposed to form two counter-propagating waves:  $p_2^i = \sum_{m=1}^{\infty} p_2^{i_m}$  and  $p_2^o = \sum_{m=0}^{\infty} p_2^{o_m}$ . Because the reflecting wall presents a velocity node, these two wave components in front of the reflecting wall must be equal in magnitude but different in phase by  $2\delta = 2k_0s$  at the position of membrane, i.e.,

$$|p_2^i| = |p_2^o|, \quad p_2^i/p_2^o = \exp(2i\delta).$$

Here  $k_0$  denotes the sound's wavevector in air, and  $s$  is the air layer's thickness.

As the conservation of MCPA is valid for membrane's each scattering, it also holds for their superpositions—the total wave field on the membrane. Therefore,  $(p_1^i + p_2^i)/2 = (p_1^o + p_2^o)/2$ , where  $p_1^o = \sum_{m=0}^{\infty} p_1^{o_m}$  is also a superposition for outgoing waves on the left-hand side after each scattering. Assuming the incoming energy is completely absorbed by the DMR, there will be no reflection on the incident side, thus  $p_1^o = 0$ . Thus the conservation of MCPA,  $p_1^i = p_2^o - p_2^i$ , may be represented by a phasor-diagram, shown in Fig. 6(b), which is an isosceles triangle with  $p_2^i$  and  $p_2^o$  being the two equal sides and  $p_1^i$  being the base. It is clear from the diagram that  $p_2^i + p_2^o$ , which is the right-hand side pressure on the DMR, differs from the left-hand side pressure,  $p_1^i$ , by a phase of  $\pi/2$ . That is,  $p_2^i + p_2^o$  is perpendicular to  $p_1^i$  in the phasor-diagram, so that  $p_2^i + p_2^o = ip_1^i \cot \delta$ . Since the surface-averaged velocity is given by  $\langle \dot{W} \rangle = \langle \dot{W}_1 \rangle = p_1^i/Z_0$ , the total pressure applied to the DMR,  $\langle p_{\text{tot}} \rangle = p_1^i - (p_2^i + p_2^o)$ , is given by  $\langle p_{\text{tot}} \rangle = p_1^i(1 - i \cot \delta)$ . It follows that the impedance condition for achieving total absorption is given by

$$Z = \langle p_{\text{tot}} \rangle / \langle \dot{W} \rangle = Z_0(1 - i \cot \delta). \quad (9)$$

For  $\delta = \pi/2$ , we have  $Z = Z_0$ , i.e., impedance matching. Such condition occurs at the sealed cell's "drum" resonances when  $s = (N/2 + 1/4)\lambda$ , with  $N$  being an integer. However, for an air layer thinner than a quarter-wavelength,  $\delta \rightarrow 0$ , and the required imaginary part of  $Z$  approaches  $-i\infty$ . Such a large imaginary part of the DMR impedance is necessary in order to cancel the impedance of the reflecting back surface that is close by. Since the impedance of the whole structure is the addition of the two serial impedances of the DMR and the sealed cell behind it, the net impedance of the structure is still  $Z = Z_0$ , i.e., impedance matched to that of air [18]. In what follows, we will show that by utilizing the *hybrid mode* of the DMR, such large imaginary impedance of the DMR can indeed be realized, while maintaining the real part to be  $Z_0$ . The reason behind the large imaginary impedance is due to the existence of DMR's anti-resonance condition, realized at

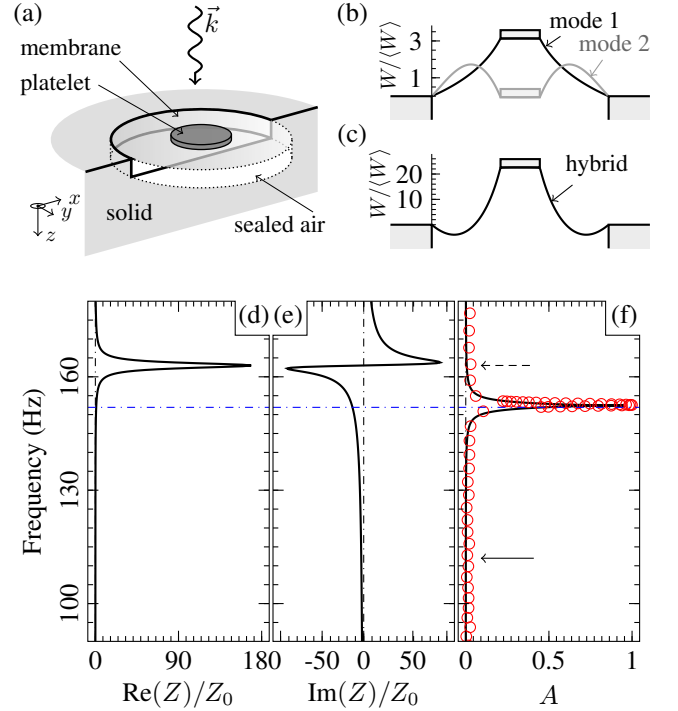


FIG. 7. The behavior of a perfect absorber for one-side incident wave, denoted the hybrid resonance metasurface. (a) Schematic illustration of the unit cell's component and geometry. (b) Schematic cross-sectional illustration of the two lowest frequency eigenmodes of the DMR, plotted in reference to the same phase of incident wave, with  $W$  being the normal displacement of membrane, normalized to its surface average component  $\langle W \rangle$ . (c) Displacement profile of the DMR's hybrid mode at 152 Hz, which is clearly a superposition of the two in (b), but with an almost an order of magnitude larger amplitude. However, such large amplitude oscillations are only coupled to the non-radiative evanescent waves, as shown in Section II. (d,e) As a function of frequency, the DMR's surface impedance  $Z$ , normalized to the impedance of air,  $Z_0$ , is seen to satisfy the total absorption requirement given by Eq. (9) at the hybrid resonance frequency, which is indicated by the blue dot-dashed line. This is confirmed experimentally measuring the absorption coefficient, shown in (f). A sharp absorption peak, reaching 0.994, is seen. The solid and dashed arrows indicate the first eigenmode and the anti-resonance frequencies of the DMR. Experimental results are shown in red circles, and black curves denote the simulation results.

frequency  $\tilde{\omega}$  that is in-between the two low-lying resonances, at which the dynamic mass density of the DMR can display a resonance-like dispersion [3].

In order to see the emergence of the hybrid mode, here for simplicity we consider only two relevant eigenmodes  $W_1$  and  $W_2$  [as shown in Fig. 7(b)], in contrast to Eq. (1), which is valid only for frequencies close to one of the DMR resonances. The surface-averaged Green function of the DMR is given by [21]

$$\langle G \rangle = \sum_{n=1}^2 \frac{|\langle W_n \rangle|^2}{\rho_n(\omega_n^2 - \omega^2)} + 2i\beta \sum_{n=1}^2 \frac{|\langle W_n \rangle|^2 \omega}{\rho_n(\omega_n^2 - \omega^2)^2} \quad (10)$$

where  $\beta$ , the averaged coefficient of  $\beta_1$  and  $\beta_2$ , is taken to be a

small quantity so that the dimensionless  $\beta/\omega \ll 1$ . We notice that in the vicinity of the DMR's anti-resonance frequency  $\tilde{\omega}$ , at which  $\text{Re}(\langle G \rangle) = 0$  (i.e.,  $Z \rightarrow \infty$ ), this surface-averaged Green function behaves as  $\langle G \rangle \simeq 2\Xi(i\beta - \Delta\omega)$ , where

$$\Xi \equiv \sum_{n=1}^2 \frac{|W_n|^2 \tilde{\omega}}{\rho_n (\omega_n^2 - \tilde{\omega}^2)^2}, \text{ and } \Delta\omega \equiv \tilde{\omega} - \omega.$$

From the inverse relationship between the Green function and impedance as describe previously, the surface impedance in the vicinity of DMR's anti-resonance is given by

$$Z = \frac{1}{2\tilde{\omega}\Xi} \frac{1}{\beta^2 + \Delta\omega^2} (\beta - i\Delta\omega). \quad (11)$$

Equating Eqs. (9) and (11) yields two equations for the condition of total absorption:

$$\frac{1}{2\tilde{\omega}\Xi} \frac{\beta}{\beta^2 + \Delta\omega^2} = Z_0, \quad (12a)$$

$$\frac{1}{2\tilde{\omega}\Xi} \frac{\Delta\omega}{\beta^2 + \Delta\omega^2} = Z_0 \cot \delta. \quad (12b)$$

This total absorption condition is robust since experimentally we have two parameters,  $\beta$  and  $\Delta\omega$ , which can be adjusted to satisfy Eq. (12). Notice that this total absorption mode of the membrane is neither of its two original DMR resonances, but a hybridization of them [as shown in Fig. 7(c)] caused by the back reflecting surface that is located in the near-field region of the DMR. Since the dissipation coefficient is required to be very small, hence to completely dissipate the incoming acoustic energy, the amplitude of this hybrid mode is always significantly larger than the original membrane's resonances for the same incident wave amplitude. This is clear from the comparison between Figs. 7(b) and (c). However, it is to be especially noted that in spite of the large maximum amplitude of the hybrid mode, the surface-averaged normal displacement is small and matches that of air.

Experiments reported in Ref. [18] have corroborated the existence and condition for this hybrid resonance total absorption. By placing an aluminum-reflecting wall behind a DMR, which is a 90 mm-wide, tensioned circular elastic membrane decorated by a 800 mg platelet with a radius of 10 mm [Fig. 7(a)], an absorption peak with  $A > 0.99$  was observed at 152 Hz [Fig. 7(f)]. By using a value of  $s = 21.7$  mm, which is inferred from the experimental data of  $s = 17$  mm of SF6 gas, as the effect of two thin gas layers is identical if their thicknesses are scaled linearly with their adiabatic index (SF6 has an adiabatic index of 1.098, compared to 1.4 for air) [18]. Based on the two relevant eigenmodes shown in Fig. 7(b), the evaluated  $\Xi = 1.268 \times 10^{-9} \text{m}^2 \text{s}^3 / \text{kg}$ ,  $\tilde{\omega} = 2\pi \times 162.3$  Hz, and  $\beta = 5.14$  Hz. Equation (11) gives the surface impedance of the DMR as a function of frequency, shown in Figs. 7(d) and 7(e). At the total absorption frequency, we have  $Z = 1.001 - 12.961i$ , which is noted to match the value required,  $Z_0(1 - i \cot(k_0 s)) = 1 - 16.342i$ , reasonably well.

## VI. CONCLUDING REMARKS

We have proposed a generalized perspective for the scattering and absorption behaviors of thin membrane structures in the subwavelength regime. As a result of DMR's negligible thickness, the conservation of MCPA for the incoming and outgoing waves can be derived. By analogy to the momentum conservation law involving two equal-mass particles, it is easy to see that within one scattering, waves incident from one side can only be absorbed by a maximum of 50%. Higher absorption requires waves incident from both sides of the DMR. Based on the Green function formalism, we determined the value of maximal absorption under different scenarios. In particular, maximal absorption is realized when the DMR has a surface impedance twice that of air. These conclusions are examined experimentally. In all cases good agreement with the theory is obtained.

For one-side incident, absorption higher than 50% can be achieved by introducing multiple scatterings, e.g., by placing a reflecting surface behind the DMR. Analysis by using the MCPA conservation law shows that near-perfect absorption can be achieved through hybrid resonances, in excellent agreement with the experimental results reported recently [18]; while at the same time it also yields the general condition [Eq (9)] for achieving such characteristic.

Due to the similarity between the acoustic and electromagnetic waves, there can clearly be analogous considerations for the latter, e.g., in laser plasma absorption [23–25]. Hence similar results are expected for electromagnetic wave scatterings from thin film structures. In particular, similarity may extend to perfect absorption by electromagnetic hybrid resonances.

## ACKNOWLEDGMENTS

J.M. and P.S. wish to thank Guoliang Huang for helpful discussions. This work is supported by Hong Kong RGC Grants AoE/P-02/12. JM is supported by the National Natural Science Foundation of China (Grant No. 11274120), and the Fundamental Research Funds for the Central Universities (Grant No. 2014ZG0032).

## Appendix A: Transmission/Reflection Retrieval Method

As scalar waves, airborne sound can propagate in a sub-wavelength waveguide without a cut-off frequency. In our experiments, the geometrical size of the apparatus (viz., the width of the square waveguide) [cf. Fig. 2 (a)] is smaller than the measured wavelength, so that only plane waves can propagate in both the front and back tubes [26]. The total pressure fields in the two (front and back) impedance tubes may be expressed as the sum of forward and backward waves propagating along the  $z$  direction:

$$p_1 = p_1^i e^{ik_0 z} + p_1^o e^{-ik_0 z}, \quad (A1a)$$

$$p_2 = p_2^i e^{-ik_0 z} + p_2^o e^{ik_0 z}. \quad (A1b)$$

Here the subscripts “1” and “2” refer to the front and back tubes and the superscripts “i” and “o” represent the incoming and outgoing waves, respectively. To retrieve the transmission and reflection coefficients, the total pressure fields should be exactly expressed, by using the four experimentally measured parameters:  $p_1^i$ ,  $p_1^o$ ,  $p_2^i$  and  $p_2^o$ . Four sensors are used to determine these parameters. Two sensors labeled “1” and “2” are placed in the front tube at  $z_1 = -339.5$  mm and  $z_2 = -239.5$  mm, and the other two sensors labeled “3” and “4” are placed in the back tube at  $z_3 = 193.0$  mm and  $z_4 = 393.0$  mm [cf. Fig. 2 (a)]. According to Eq. (A1), the pressure values at the positions of the four sensors are

$$p(z_1) = p_1^i e^{ik_0 z_1} + p_1^o e^{-ik_0 z_1}, \quad (\text{A2a})$$

$$p(z_2) = p_1^i e^{ik_0 z_2} + p_1^o e^{-ik_0 z_2}, \quad (\text{A2b})$$

$$p(z_3) = p_2^i e^{-ik_0 z_3} + p_2^o e^{ik_0 z_3}, \quad (\text{A2c})$$

$$p(z_4) = p_2^i e^{-ik_0 z_4} + p_2^o e^{ik_0 z_4}. \quad (\text{A2d})$$

By solving Eq. (A2), we obtain

$$p_1^i = \frac{p(z_1)e^{ik_0 z_1} - p(z_2)e^{ik_0 z_2}}{e^{2ik_0 z_1} - e^{2ik_0 z_2}}, \quad (\text{A3a})$$

$$p_1^o = -\frac{p(z_1)e^{ik_0 z_2} - p(z_2)e^{ik_0 z_1}}{e^{2ik_0 z_1} - e^{2ik_0 z_2}} e^{ik_0(z_1+z_2)}, \quad (\text{A3b})$$

$$p_2^i = -\frac{p(z_3)e^{ik_0 z_4} - p(z_4)e^{ik_0 z_3}}{e^{2ik_0 z_3} - e^{2ik_0 z_4}} e^{ik_0(z_3+z_4)}, \quad (\text{A3c})$$

$$p_2^o = \frac{p(z_3)e^{ik_0 z_3} - p(z_4)e^{ik_0 z_4}}{e^{2ik_0 z_3} - e^{2ik_0 z_4}}, \quad (\text{A3d})$$

Here  $p(z_j)$  is the pressure measured by each sensor labeled as “ $j = 1 \sim 4$ ” in the subscripts.

The scattering matrix  $S(k_0)$  describing the relationship between the incoming and outgoing waves can be expressed as

$$\begin{pmatrix} p_2^o \\ p_1^o \end{pmatrix} = S(k_0) \begin{pmatrix} p_1^i \\ p_2^i \end{pmatrix}, \quad S(k_0) = \begin{pmatrix} T & R \\ R & T \end{pmatrix}. \quad (\text{A4})$$

It should be noted that, due to the symmetry of the sample in our system, the reflection and transmission coefficients  $R$  and  $T$  are identical if the sample is tuned around 180 degrees. As a result, the reflection and transmission coefficients can be retrieved as

$$R = \frac{p_1^i p_1^o - p_2^i p_2^o}{p_1^i p_1^i - p_2^i p_2^i}, \quad (\text{A5a})$$

$$T = \frac{p_1^i p_2^o - p_1^o p_2^i}{p_1^i p_1^i - p_2^i p_2^i}. \quad (\text{A5b})$$

Here the four wave amplitude  $p_1^i$ ,  $p_1^o$ ,  $p_2^i$  and  $p_2^o$  are determined from Eq. (A3).

- 
- [1] J. P. Arenas and M. J. Crocker, *Sound & vibration* **44**, 12 (2010).
- [2] H. V. Fuchs and X. Zha, *Acta acustica united with acustica* **92**, 139 (2006).
- [3] Z. Yang, J. Mei, M. Yang, N. Chan, and P. Sheng, *Physical review letters* **101**, 204301 (2008).
- [4] Z. Yang, H. Dai, N. Chan, G. Ma, and P. Sheng, *Applied Physics Letters* **96**, 041906 (2010).
- [5] C. J. Naify, C.-M. Chang, G. McKnight, and S. Nutt, *Journal of Applied Physics* **110**, 124903 (2011).
- [6] G. Ma, M. Yang, Z. Yang, and P. Sheng, *Applied Physics Letters* **103**, 011903 (2013).
- [7] Y. Chen, G. Huang, X. Zhou, G. Hu, and C.-T. Sun, *The Journal of the Acoustical Society of America* **136**, 969 (2014).
- [8] J. J. Park, K. Lee, O. B. Wright, M. K. Jung, and S. H. Lee, *Physical Review Letters* **110**, 244302 (2013).
- [9] S. H. Lee, C. M. Park, Y. M. Seo, and C. K. Kim, *Physical Review B* **81**, 241102 (2010).
- [10] C. M. Park, J. J. Park, S. H. Lee, Y. M. Seo, C. K. Kim, and S. H. Lee, *Physical review letters* **107**, 194301 (2011).
- [11] S. H. Lee, C. M. Park, Y. M. Seo, Z. G. Wang, and C. K. Kim, *Physics Letters A* **373**, 4464 (2009).
- [12] S. H. Lee, C. M. Park, Y. M. Seo, Z. G. Wang, and C. K. Kim, *Physical review letters* **104**, 054301 (2010).
- [13] M. Yang, G. Ma, Z. Yang, and P. Sheng, *Physical review letters* **110**, 134301 (2013).
- [14] J. Mei, G. Ma, M. Yang, Z. Yang, W. Wen, and P. Sheng, *Nature communications* **3**, 756 (2012).
- [15] Y. Chen, G. Huang, X. Zhou, G. Hu, and C.-T. Sun, *The Journal of the Acoustical Society of America* **136**, 2926 (2014).
- [16] J. de Rosny and M. Fink, *Physical review letters* **89**, 124301 (2002).
- [17] A. Derode, P. Roux, and M. Fink, *Physical review letters* **75**, 4206 (1995).
- [18] G. Ma, M. Yang, S. Xiao, Z. Yang, and P. Sheng, *Nature materials* (2014).
- [19] Y. Chong, L. Ge, H. Cao, and A. D. Stone, *Physical review letters* **105**, 053901 (2010).
- [20] L. Landau and E. Lifshitz, “Fluid mechanics,” (Pergamon Press, 1970) Chap. 8, p. 255.
- [21] M. Yang, G. Ma, Y. Wu, Z. Yang, and P. Sheng, *Physical Review B* **89**, 064309 (2014).
- [22] L. Landau and E. Lifshitz, “Theory of elasticity,” (Pergamon Press, 1970) Chap. 5, p. 153.
- [23] R. Godwin, *Physical Review Letters* **28**, 85 (1972).
- [24] J. Freidberg, R. Mitchell, R. L. Morse, and L. Rudinski, *Physical Review Letters* **28**, 795 (1972).
- [25] J. Kindel, K. Lee, and E. Lindman, *Physical Review Letters* **34**, 134 (1975).
- [26] P. M. Morse and K. U. Ingard, *Theoretical Acoustics* (Princeton University Press, Princeton, NJ, 1986).